JST: Engineering and Technology for Sustainable Development
Volume 33, Issue 4, October 2023, 032-040

Effect of Temperature on Mechanical Energy Absorption of Graphene-Based Honeycomb Structure Doped Boron and Nitrogen

Nguyen Minh Son[1], Nguyen Hoang Linh[1], Tran The Quang[2], Vuong Van Thanh[1], Do Van Truong[1,*]
[1]Hanoi University of Science and Technology, Ha Noi, Vietnam
[2] Thai Binh University, Thai Binh, Vietnam
[*]Corresponding author email: truong.dovan@hust.edu.vn

Abstract

The C_3B, C_3N, and NB-based honeycomb structures (GBNHs) are promising candidates for creating parts that can absorb energy when subjected to external forces. However, the mechanical energy absorption capacity of GBNHs can be changed significantly under different temperatures. In this study, we focus on investigating the effect of temperature on the energy absorption capacity and mechanical properties of GBNHs via molecular dynamics (MD). The obtained results show that the energy absorption capacity of GBNHs sharply increases with the decrease in temperature. At room temperature, the average mechanical energy absorption capacity of GBNHs is over about 5500 MJ/m^3 and the everage anti-penetration ability can reach over 9300 MJ/m^3. The potential of GBHNs exceed the graphene-based carbon honeycombs (GCHs) by about 5440 MJ/m^3. Besides, the temperature also affects the mechanical properties of GBNHs. The critical strain is decreased with increasing temperature. These obtained results provide important bases for GBNH in the production of energy-absorbing components.

Keywords: Temperature effect, graphene-based carbon honeycombs, energy absorption materials, stress-strain curves, molecular dynamics.

1. Introduction

Mechanical energy absorption materials such as cast-iron, steel, and foam [1- 3] have been widely used. Interestingly, nature has provided energy absorption materials (EAM) such as bones [4] and nacre [5], which have inspired the development of novel materials with greater energy absorption capacities, such as steel foam with a mechanical energy absorption capacity of about 183.23 MJ/m^3 [2]. However, these energy absorption capacities may not be sufficient for the urgent needs of the current industry. In recent research, honeycomb-structured materials have emerged as a promising area of study. Of particular interest is the structure of graphene-based carbon honeycombs (GCHs) [1, 3], which have been successfully synthesized in the laboratory. GCHs possess outstanding mechanical and thermal properties [6, 7]. GCHs are made of monolayer graphene sheets that are spread along the *z*-direction and connected via sp^3 bonds. Due to their special structure, the mechanical energy absorption capacity of GCHs increases with a large strain range [6], and can reach 5440MJ/m^3, which is equivalent to the absorption capacity of graphene and 10 times greater than that of steel sheets. Furthermore, new 2D materials based on the graphene structure have emerged, where carbon (C) atoms are replaced by nitrogen (N) [8] and boron (B) [9] atoms in the ratios of 3:1 (C:B/N) or all carbon atoms are replaced by two atoms as boron-nitrogen [10]. Studies have shown that monolayer sheets such as C_3B and C_3N possess high critical stresses of about 125GPa [9] and about 130GPa [8], respectively.

Currently, many studies have concentrated on the mechanical and thermal properties of the honeycomb structures based on graphene [6]. The studies have proved that temperature has a significant effect on the mechanical properties such as the maximum stress and fracture strain [11-14]. The material GCHs [6] has the critical stress and fracture strain at room temperature about 30 GPa and 20%, respectively, and the mechanical absorbing coefficient coming up 5440 MJ/m^3. At 900 K, the mechanical properties express a slight change [7], but at a temperature of 1800 K the critical stress has sharp adjustment, it decreases about 70%. Besides, the mechanical energy absorbing coefficient also declines about 80%. Thus, the high temperature is demonstrated to have a significant impact on the mechanical properties of the materials. They are more easily destroyed and their mechanical energy absorbing coefficient is also changed remarkably. Recently, the graphene sheets doped with boron and nitrogen-based honeycomb structures (GBNHs) have attracted attention owing to having the analogous structure to GCHs. In this study, we aim to investigate the effect of temperature on the mechanical properties and energy absorption capacity of

ISSN 2734-9381
https://doi.org/10.51316/jst.169.etsd.2023.33.4.5
Received: March 7, 2023; accepted: August 9, 2023

graphene-based boron-nitrogen honeycomb structures (we have used these terms C_3NHs, C_3BHs and NBHs for the C_3N, C_3B and NB based honeycomb structures). To achieve their properties, we employ molecular dynamics (MD) as a simulation tool to analyze the relationship between stress and strain of GBNHs structures at different temperatures. Our findings could provide valuable insights into the potential use of GBNHs materials in the future.

2. Methodology

The model of GBNHs was constructed using hexagonal cells, and periodic boundary conditions were imposed in all three directions. Each hexagonal cell was formed from six monolayer graphene sheets doped with boron and nitrogen (Fig. 1). The atoms were connected to each other through sp^2 bonds. The simulations in the x and y directions were considered to be in-plane, while that in the z direction was out-of-plane. The models have been carefully tested with different parameters, the most optimal parameters, that simultaneously help reduce simulating time and produce the most dependable results are lx = 200Å, ly = 200Å, and lz = 50Å for the in-plane, and lx= ly = 70Å and lz = 110Å for the out-of-plane.

The software LAMMPS [15] was used to perform simulations in this study. The interactions between carbon, nitrogen, and boron atoms in the GBNHs models were represented by the TERSOFF potential function. Moreover, some parameters of the potential function were adjusted as suggested by Kinaci *et al* [16] are listed in Table 1.

$$V_{ij} = f_{ij}^{c}\left(a_{ij}.f_{ij}^{R} - b_{ij}.f_{ij}^{A}\right) \quad (1)$$

$$f_{ij}^{R} = A.e^{-\lambda_1.r_{ij}} \quad (2)$$

$$f_{ij}^{A} = B.e^{-\lambda_2.r_{ij}} \quad (3)$$

where r_{ij} is the distance between atoms i and j, f_{ij}^{A} and f_{ij}^{R} are competing attractive and repulsive pairwise terms, and f_{ij}^{C} is a cutoff term which ensures only nearest-neighbor interactions. The term, a_{ij}, is a range-limiting term on the repulsive potential that is typically set equal to 1.

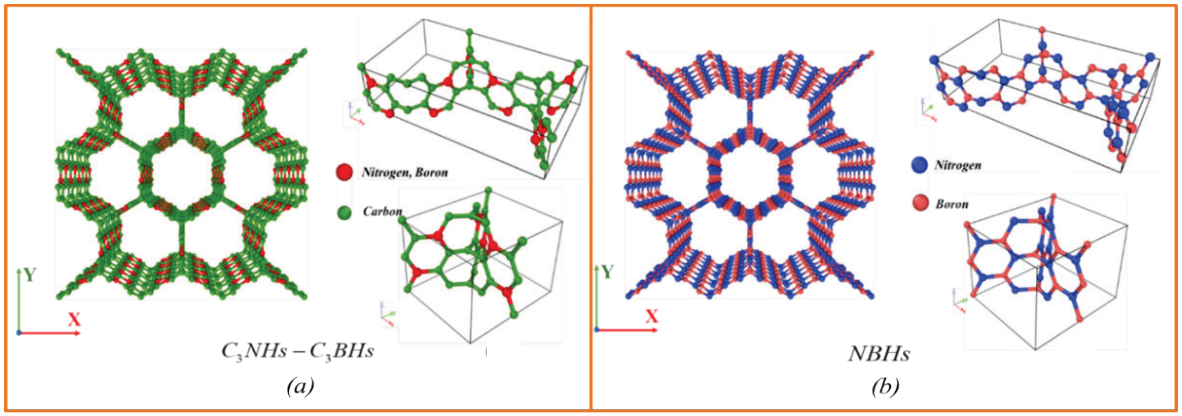

Fig. 1. The predicted models and the structure of the unit cell and the atom structure of a junction among the walls C_3BHs, C_3NHs *(a)*, and NBHs *(b)*.

Table 1. The optimal parameters of Tersoff potential for GBNHs materials.

Parameters	C B	C C	C N	B C	B N	N B	N C
A	1386.78	1393.6	1386.78	1386.78	1380	1380	1386.78
B	339.0689	430	387.5752	339.0689	340	340	387.5752
λ_1	3.5279	3.4879	3.5279	3.5279	3.568	3.568	3.5279
λ_2	2.2054	2.2119	2.2054	2.2054	2.199	2.199	2.2054
$\lambda 3$	0.000	0.000	0.000	0.000	0.000	0.000	0.000
n	0.72751	0.72751	0.72751	0.72751	0.72751	0.72751	0.72751
β	1.5724	1.5724	1.5724	1.25724	1.25724	1.25724	1.25724
c	38049	38049	38049	25000	25000	25000	25000
d	4.3484	4.3484	4.3484	4.3484	4.3484	4.3484	4.3484
h	−0.93	−0.93	−0.93	−0.89	−0.89	−0.89	−0.89
R	1.85	1.8	1.85	1.85	1.9	1.9	1.85

The bond angle term, b_{ij}, depends on the local coordination of atoms around atom *i* and the angle between atoms *i, j*, and *k*.

$$b_{ij} = \left(1+\beta^n.\zeta_{ij}^n\right)^{-\frac{1}{2n}} \quad (4)$$

$$\zeta_{ij}^n = \sum_{k\neq ij} f_{ik}^C \cdot g_{ijk} e^{\lambda_3^3\cdot\left(r_{ij}-r_{jk}\right)^3} \quad (5)$$

$$g_{ijk} = 1+\frac{c^2}{d^2}-\frac{c^2}{d^2+\left(h-\cos\left(\theta_{ijk}\right)\right)^2} \quad (6)$$

where θ_{ijk} is the angle between atoms *i, j*, and *k*. and *d, c, h* are the adjustable parameters.

In order to control temperature, the study used the Nose-Hoover thermostat equations. Before applying tensile and compressive strains, the models were equilibrated with the isothermal-isobaric (NPT) ensemble using the Nose-Hoover thermostat and barostat. A time step of 0.75 fs, an equilibration time of 7.5 ns, and a stress condition of less than 0.01 MPa were used. The canonical (NVT) ensemble in compressive and tensile strains had a strain rate of 0.001 ps^{-1}. The elastic modulus *E* was calculated as follows:

$$E = \frac{\sigma}{\varepsilon} \quad (7)$$

where the stress σ was taken at the small strain ε (about 1%). The energy absorption per unit volume W_v and the energy absorption per unit mass W_m [2, 16, 17] were calculated using the formulas:

$$W_v = \int_{\varepsilon_0}^{\varepsilon_1} \sigma d\varepsilon \,; W_m = \frac{W_v}{\rho} \quad (8)$$

where the coefficient ρ is the mass density of the respective structures.

3. Results and Discussion

3.1. In-Plane

In fact, the energy absorption capacity of the honeycomb structure is calculated based on the stress-strain relationship in the *x* and *y* directions (in-plane). Through (7), we have calculated the elastic modulus for C_3NHs, C_3BHs and NBHs in both *x* and *y* directions that are 145 GPa, 138 GPa and 153 GPa, for *x* direction and 150 GPa, 137 GPa and 158 GPa for *y* direction, respectively that are consistent with the previous studies [18, 19].

Fig. 2 depicts the effect of temperature on the tensile stress-strain curves in the in-plane. In general, at room temperature, all structures can withstand a fracture strain higher than about 18%, especially the NBHs can endure a fracture strain greater than about 60%. In the early stage, the temperature has an insignificant effect on the stress. However, toward the end of the stage, with the increase in temperature, the fracture strain and the critical stress of three structures remarkably decline in both *x* and *y* directions. At 100 K, the NBHs possess critical stresses of 225 GPa and 180 GPa at the fracture strain of 81.6% and 71.5% (Fig. 2*b*) in the *x* and *y* directions, respectively. At a temperature of 900 K, the fracture strain of NBHs decreases by 50% and 59% in the *x* and *y* directions, respectively, while the critical stress declines by a factor of three compared to that at 100 K in both directions. In terms of C_3NHs and C_3BHs, at 100 K, there is a similar value of the critical stresses, about 36 GPa, in both structures. In addition, the fracture strains of C_3NHs that are correspondingly 30% and 24% in *x* and *y* directions are lower than that of C_3BHs (at 33% and 35% respectively). At a temperature of 900 K, the critical stress of C_3NHs decreases by 65% compared to that at 100K, whereas the critical stress reduction of C_3BHs is about 56%. In addition, temperature affects the fracture strain of both structures, with the fracture strain of both C_3NHs and C_3BHs decreasing by half at 900 K compared to that at 100K. This change occurs because the bonds can be weaker with the increase of temperature, and the vibration of bonds is more intense, owing to larger thermal fluctuations at higher temperatures [20]. Temperature increases with the decrease in the stability of the atoms' bonds, leading to the fracture of structures which occurs more quickly than at lower temperatures. The same response is observed in other structures, such as graphene doped boron, nitrogen [8, 9], and GCHs [7].

The obtained results under compressive strain in the *x* and *y* directions are shown in Fig. 3. The compressive process can be classified into four major stages [6], with stage I being linear elastic, where stress increases linearly in a short range of strain. After stress reaches a certain value at the end of stage I, it fluctuates around this value in a large strain range, which is considered as the stress plateau stage (stage II). Stage III is the hardening stage where stress grows dramatically, and the final stage (IV) is the densification stage. In the early stages (I, II), temperature has an insignificant effect on stress. However, the strain of stage II decreases with increasing temperature, as does the strain of stage III.

Table 2 shows the influence of temperature on the strains of stages II and III. The energy absorption capacities of GBNHs are determined based on the stress-strain relationship in stages II and III in-plane. In stage II, the stress of C_3NHs, C_3BHs, and NBHs fluctuates around 5 GPa, 4 GPa, and 2.5 GPa, respectively. Due to their unique structures, the hexagonal cells in these structures contain a large vacuum (as shown in Fig. 1*a*). Under compressive strain in the *x* and *y* directions, the vacuum in the cells narrows consecutively, leading to the stress of GBNHs only fluctuating around a certain value.

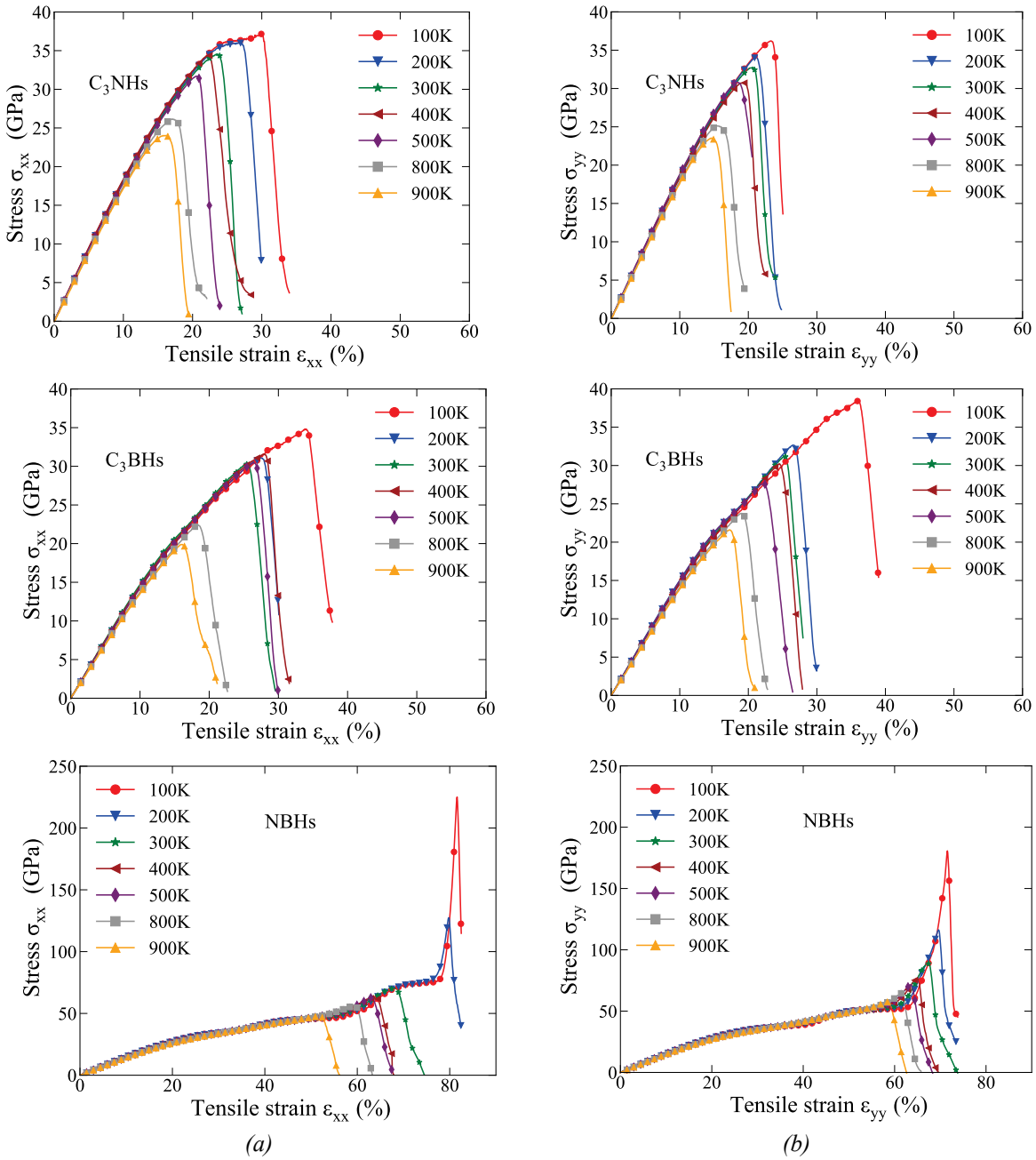

Fig. 2. The tensile stress-strain curves of C_3NHs; C_3BHs; NBHs in *x (a)* and *y (b)* directions.

Table 2. The end strain value of two stages II and III in the compressive process in *x, y* directions at different temperatures.

	100K	200K	300K	400K	500K	800K	900K
C_3N-II	0.550	0.500	0.450	0.440	0.420	0.400	0.385
C_3B-II	0.540	0.490	0.450	0.435	0.430	0.400	0.350
NB-II	0.580	0.520	0.480	0.450	0.445	0.420	0.400
C_3N-III	0.685	0.670	0.650	0.645	0.630	0.625	0.610
C_3B-III	0.690	0.675	0.650	0.645	0.630	0.620	0.615
NB-III	0.720	0.700	0.680	0.670	0.665	0.640	0.620

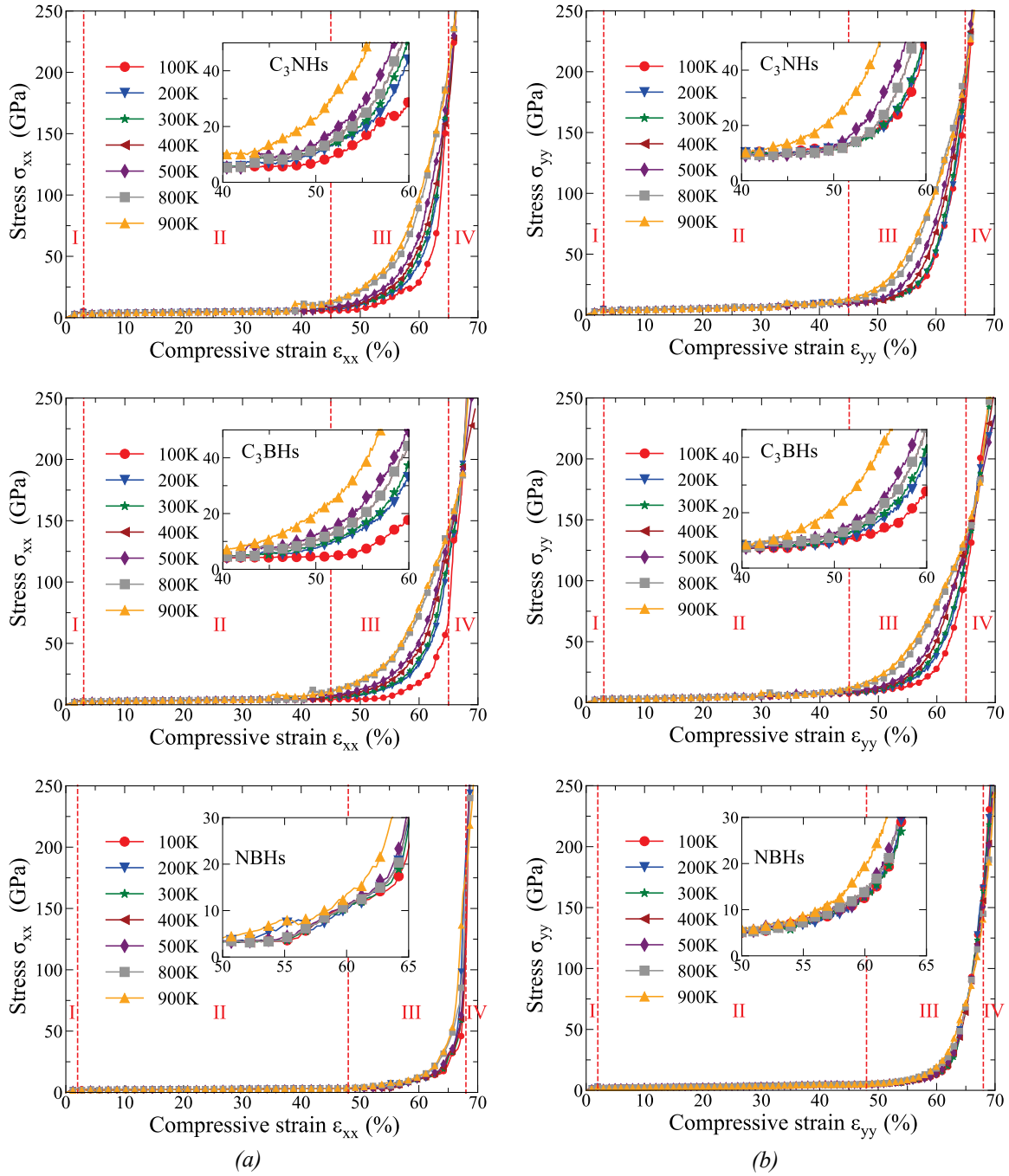

Fig. 3. The compressive stress-strain curves of C_3NHs, C_3BHs, NBHs in *x (a)* and *y (b)* directions respectively.

Stage III can be divided into two substages (III-a and III-b). In stage III-a, the distance between cell walls decreases with increasing compressive strain in the *x* and *y* directions, resulting in an increase in the Van-der-waal formed from wall-wall interaction. This special interaction causes a slight increase in stress in stage III-a. When the distance between cell walls is under the equilibrium distance (3.4Å), the Van-der-Waals interaction becomes attractive (stage III-b). In addition, densification areas appear in the structures in stage III-b, which is similar to previous studies [6,7]. The energy absorption capacities of structures in stages II and III at room temperature (300K) are listed in Table 3. Compared to the GCHs in the previous study [6], the mechanical energy absorbing capacity of GCHs is lower than that of GBNHs at room temperature (Table 3).

Table 3. The energy absorption capacity of the stage II and III in the *x, y* directions of the GBNHs structures and GCHs at the room temperature of 300K.

Materials	W_v (MJ/m^3)	W_m (J/g)	Strain (%)	Reference
GCHs-*x*	780	532	0.39	[6]
GCHs-*y*	950	647	0.39	[6]
GCHs-III-*x*	5440	3710	0.63	[6]
GCHs-III-*y*	5820	3963	0.63	[6]
C_3B-*x*	1687	1097	0.45	This article
C_3B-*y*	2082	1353	0.45	…
C_3B-III-*x*	5728	3723	0.65	…
C_3B-III-*y*	6059	3938	0.65	…
C_3N-*x*	2115	1480	0.45	…
C_3N-*y*	2683	1878	0.45	…
C_3N-III-*x*	8079	5655	0.65	…
C_3N-III-*y*	8531	5971	0.65	…
NB-*x*	1226	858	0.48	…
NB-*y*	1549	1084	0.48	…
NB-III-*x*	5130	3591	0.68	…
NB-III-*y*	5877	4114	0.68	…

Table 4. The energy absorption per unit volume - W_v (MJ/m^3) in the *x, y* directions of the C_3NHs, C_3BHs, NBHs structures at different temperatures.

			100K	200K	300K	400K	500K	800K	900K
C_3NHs	*x*	II	2919	2516	2115	1830	1817	1691	1599
		III	11219	9177	8079	7075	6952	5905	5350
	y	II	3917	3235	2683	2546	2330	2178	2068
		III	11581	10550	8531	8231	7548	6163	5542
C_3BHs	*x*	II	2255	2198	1687	1649	1577	1447	1363
		III	8772	8590	5728	5160	4862	4499	4126
	y	II	2752	2470	2082	1911	1871	1754	1632
		III	9052	8314	6059	5342	4542	4055	3871
NBHs	*x*	II	1547	1460	1226	1160	1079	1011	995
		III	8577	7230	5130	4960	4570	2860	1967
	y	II	2138	2043	1549	1460	1365	1244	1154
		III	9769	7650	5877	4600	3729	3729	2142

However, the mechanical stability of GCHs [7] appears to be higher than that of GBNHs under various temperatures because graphene can withstand higher temperatures than monolayers of C_3B, C_3N, and NB [10]. The study investigates the effect of temperature on the energy absorption capacity per unit volume W_v of GBNHs in stages II and III (Table 4). Through these results, the study shows that temperature has an enormous effect on the energy absorption capacity of GBNHs, and stress and strain are the two major factors affecting the energy absorption capacity. Thus, when materials experience thermal impacts, it directly affects their mechanical energy absorption capacity.

3.2. Out-of-Plane

The mechanical energy absorption capacity calculated in the *z* direction of honeycomb structures is a major factor in determining their anti-penetration ability, which is important for applications such as bulletproof vests. Based on (7), the calculated elastic modulus of C_3NHs, C_3BHs and NBHs are 514 GPa, 488 GPa, and 382 GPa, respectively. Fig. 4*a* shows the stress-strain curves of GBNHs under tensile strain in the *z* direction at different temperatures ranging from 100K to 900K. In the early stages, the temperature has an insignificant effect on stress. However, at the fracture stage, the critical stress and fracture strain of

the structures decrease with increasing temperature. Compared to CNTs and GCHs, which are the structures most similar to GBNHs composed of many hexagonal cells, the study has shown that GBNHs have higher stress than GCHs [6] but lower stress than CNT [21] when subjected to tensile strain in the *z* direction. This is due to the weaker carbon-nitrogen and boron bonds compared to sp^2 carbon-carbon bonds, while the sp^3 carbon-carbon bonds are weaker than carbon-nitrogen and boron bonds. At a temperature of 100K, NBHs have the highest critical stress at 144GPa, while C_3NHs and C_3BHs have stresses of approximately 59GPa. The fracture strains of all three structures exceed about 20%. At 900K, the critical stresses of C_3NHs and NBHs decrease by about 37%, while that of C_3BHs decreases by about 48% compared to the critical stress at 100K. The fracture strains of the structures also decrease with increasing temperature. In particular, the fracture strains of C_3BHs and C_3NHs at 900K decrease by half compared to the value at 100K, while that of NBHs only decreases by about 10%.

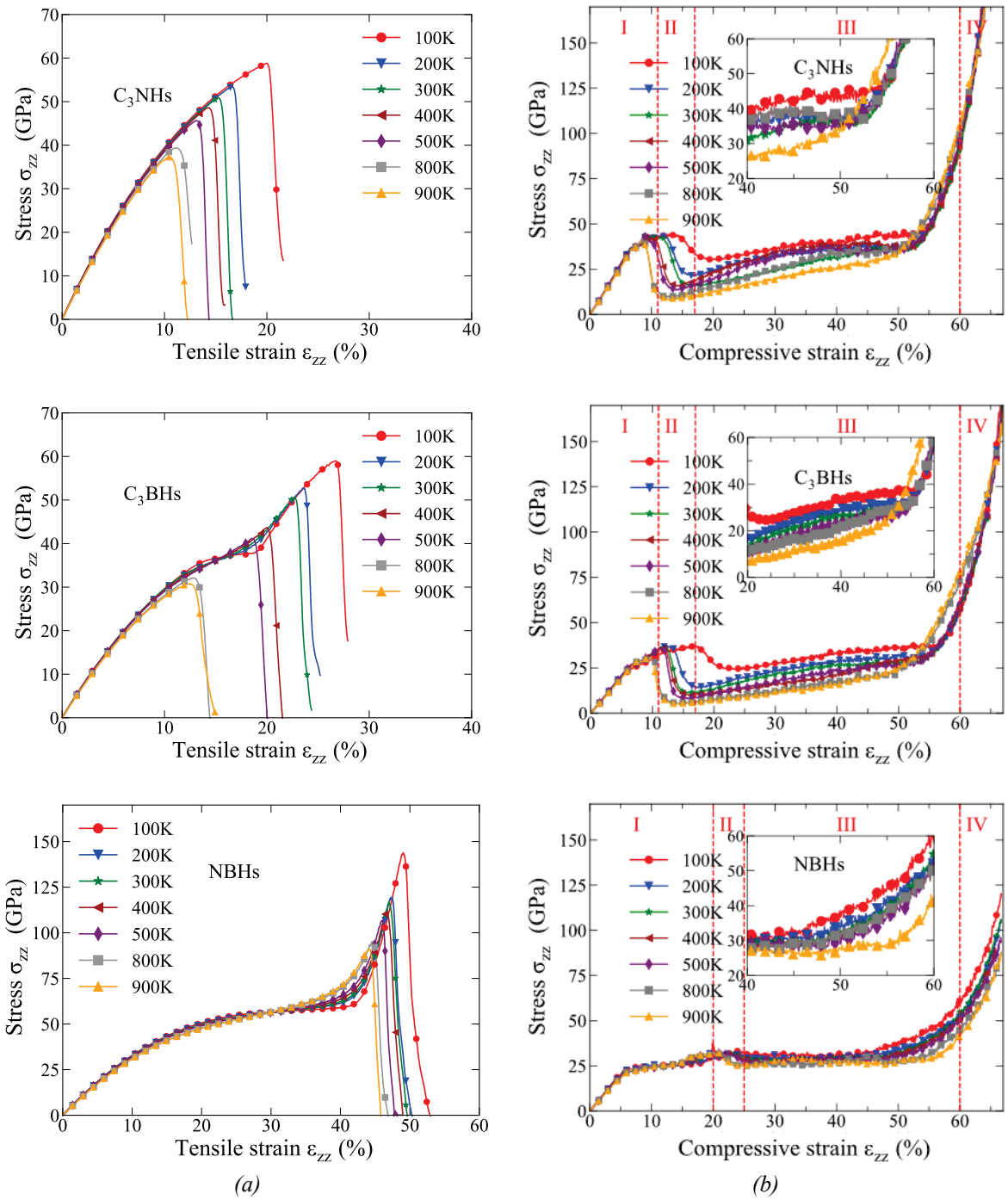

(a) *(b)*

Fig. 4. The tensile *(a)* and compressive stress *(b)*-strain curves of C_3NHs, C_3BHs, NBHs in *z* direction

Table 5. The energy absorption per unit volume-W_v (MJ/m^3) in the z direction of the C_3NHs, C_3BHs, NBHs structures at different temperatures.

	100K	200K	300K	400K	500K	800K	900K
NBHs	9785	9593	9345	9312	9180	9021	8959
C_3BHs	12408	11139	9901	8104	7903	5203	4901
C_3NHs	16112	15059	12476	12184	11416	9061	8847
GCHs	…	…	5000	…	…	…	…

The stress-strain curves of GBNHs under compressive strain in the z direction is shown in Fig. 4*b*. This compression process can be divided into four stages: linear elastic stage (I), buckling stage (II), plateau stage (III), and densification stage (IV). In stage I, the effect of temperature on stress is not significant. However, temperature has a violent influence on stress in phase II. As temperature increases, critical stress and strain decrease simultaneously, which is similar to the effect of temperature in the x and y directions. In stage III, the effect of temperature on stress is similar to that of stage II, and is negligible in stage IV.

Table 5 illustrates the effect of temperature on the penetration energy absorption capabilities per unit volume W_v. The study compares the anti-penetration ability of GBNHs with that of other materials studied previously at room temperature (300K), such as GCHs with W_v of approximately 5000 MJ/m^3 [6], and steel with approximately 4760 MJ/m^3 [2]. The mechanical energy absorption capacity per unit volume of GBNHs at room temperature is much larger than that of these materials studied previously. Therefore, GBNHs possess outstanding anti-penetration ability at present.

4. Conclusion

Through molecular dynamics simulation, this study has investigated the mechanical properties of GBNHs. The results have demonstrated that GBNHs possess exceptional energy absorption capacity and anti-penetration ability at room temperature (300K), outperforming GCHs and other materials currently available. However, it should be noted that the mechanical stability of GBNHs under different temperatures still cannot surpass that of GCHs. Additionally, the energy absorption capacity and anti-penetration ability of GBNHs decrease with increasing temperature. This study provides crucial information about the effect of temperatures on the mechanical properties and energy absorbing coefficient of GBNHs, indicating that these potentials of GBNHs can be changed in distinct temperature environments. These findings offer valuable knowledge for the future development and application of GBNHs as a mechanical energy absorption material in the industry.

Reference

[1] Wei, F. Yang, K. Bi, J. Yang, and Y. Chen, Thermal transport properties of all-sp^2 three-dimensional graphene, Anisotropy, size and pressure effects, Carbon, vol. 113, pp. 212-218. 2017. https://doi.org/10.1016/j.carbon.2016.11.055.

[2] G. Castro and S. R. Nutt, Synthesis of syntactic steel foam using gravity-fed infiltration, Materials Science and Engineering: A, vol. 553, pp. 89-95. 2012. https://doi.org/10.1016/j.msea.2012.05.097.

[3] N. V. Krainyukova, E. N. Zubarev, Carbon honeycomb high capacity storage for gaseous and liquid species, Physical Review Letters, vol. 116, no. 5, pp. 055501. 2016. https://doi.org/10.1103/PhysRevLett.116.055501.

[4] K. J. Koester, J. W. Ager, 3rd, and R. O. Ritchie, The true toughness of human cortical bone measured with realistically short cracks, Nat Mater, vol. 7, no. 8, pp. 672-677, Aug. 2008, https://doi.org/10.1038/nmat2221.

[5] Z. Tang, N. A. Kotov, S. Magonov, and B. Ozturk, Nanostructured artificial nacre, Nat Mater, vol. 2, no. 6, pp. 413-418, Jun. 2003, https://doi.org/10.1038/nmat906.

[6] L. Yi, T. Chang, X. Q. Feng, Y. Zhang, J. Wang, and B. Huang, Giant energy absorption capacity of graphene-based carbon honeycombs, Carbon, vol.118, pp.348-357.2017. https://doi.org/10.1016/j.carbon.2017.03.070.

[7] J. Hu, J. Zhou, A. Zhang, L. Yi, and J. Wang, Temperature dependent mechanical properties of graphene-based carbon honeycombs under tension and compression, Physics Letters A, vol. 391, pp. 127130. 2021. https://doi.org/10.1016/j.physleta.2020.127130.

[8] A. H. N. Shirazi, R. Abadi, M. Izadifar, N. Alajlan, and T. Rabczuk, Mechanical responses of pristine and defective C3N nanosheets studied by molecular dynamics simulations, Computational Materials Science, vol. 147, pp. 316-321. 2018. https://doi.org/10.1016/j.commatsci.2018.01.058.

[9] R. K. Zahedi, A. H. N. Shirazi, P. Alimouri, N. Alajlan, and T. Rabczuk, Mechanical properties of graphene-like BC3; a molecular dynamics study, Computational Materials Science, vol. 168, pp.1-10. 2019. https://doi.org/10.1016/j.commatsci.2019.05.053

[10] Y. Lin and J. W. Connell, Advances in 2D boron nitride nanostructures: nanosheets, nanoribbons, nanomeshes, and hybrids with graphene, Nanoscale, vol. 4, no. 22, pp. 6908-6939, Nov. 2012, https://doi.org/10.1039/c2nr32201c.

[11] T. T. Liu, X. Wang, Dynamic elastic modulus of single-walled carbon nanotubes in different thermal environments, Physics Letters A, vol. 365, pp. 144-148. 2007. https://doi.org/10.1016/j.physleta.2006.12.059.

[12] Wei, Chenyu; Cho, Kyeongjae; Srivastava, Deepak. Tensile strength of carbon nanotubes under realistic temperature and strain rate, Physical Review B, vol. 67, no. 11, pp. 115-407. 2003. https://doi.org/10.1103/PhysRevB.67.115407.

[13] Shen, Le; Shen, Hui-Shen; Zhang, Chen-Li, Temperature-dependent elastic properties of single layer graphene sheets, Materials & design, vol. 31, no. 9, pp. 4445-4449. 2010. https://doi.org/10.1016/j.matdes.2010.04.016.

[14] Zhao, Huijuan; Aluru, Narayana R, Temperature and strain-rate dependent fracture strength of graphene. Journal of Applied Physics, vol. 108, no. 6. 2010. https://doi.org/10.1063/1.3488620.

[15] Plimpton, Steve, Fast parallel algorithms for short-range molecular dynamics, Journal of computational physics, vol. 117, pp 1-19. 1995. https://doi.org/10.1006/jcph.1995.1039.

[16] A. Kınacı, J. B. Haskins, C. Sevik, and T. Çağın, Thermal conductivity of BN-C nanostructures, Physical Review B, vol. 86, no. 11. 2012. https://doi.org/10.1103/PhysRevB.86.115410.

[17] A. Han, V. K. Punyamurthula, W. Lu, and Y. Qiao, Deformation of a nanoporous silica under compressive loading, Journal of Applied Physics, vol. 103, no. 8. 2008. https://doi.org/10.1063/1.2909976.

[18] Xie, Lu, *et al*, Molecular dynamics simulation on mechanical and piezoelectric properties of boron nitride honeycomb structures, Nanomaterials, vol. 9, no. 7, pp. 1044. 2019. https://doi.org/10.3390/nano9071044.

[19] Zhang, Jin, Boron nitride honeycombs with superb and tunable piezopotential properties, Nano Energy, vol. 41, pp. 460-468. 2017. https://doi.org/10.1016/j.nanoen.2017.10.005.

[20] L. Yi, Z. Yin, Y. Zhang, and T. J. C. Chang, A theoretical evaluation of the temperature and strain-rate dependent fracture strength of tilt grain boundaries in graphene, Carbon, vol. 51, pp. 373-380. 2013. https://doi.org/10.1016/j.carbon.2012.08.069.

[21] T. T. Liu and X. Wang, Dynamic elastic modulus of single-walled carbon nanotubes in different thermal environments, Physics Letters A, vol. 365, no. 1-2, pp. 144-148.2007. https://doi.org/10.1016/j.physleta.2006.12.059.